International Journal of Nanomedicine

Dovepress
Taylor & Francis Group

Open Access Full Text Article

ORIGINAL RESEARCH

Chitosan Nanoparticles for Pulmonary Delivery of Curcumin/Nintedanib to Treat Pulmonary Fibrosis

Mengya Jin[1,*], Jinming Liu[1,*], Mengliu Shao[1], Shaoqin He[1], Yue He[2], Qingliang Yang[1], Gensheng Yang[1]

[1]College of Pharmaceutical Science, Zhejiang University of Technology, Hangzhou, 310014, People's Republic of China; [2]Pharmacy Department, Zhejiang Provincial Dermatology Hospital, Huzhou, Zhejiang, 313200, People's Republic of China

*These authors contributed equally to this work

Correspondence: Yue He; Gensheng Yang, Email hy66@zjspfb.com; yanggs@zjut.edu.cn

Background/Objective: Pulmonary fibrosis is a chronic, progressive lung disease with a high mortality rate. Currently, the treatment options for IPF involve the oral administration of nintedanib (NDNB); however, these therapies are hampered by low oral bioavailability. This study aimed to develop chitosan-based nanoparticles for pulmonary delivery to enhance the therapeutic effects of curcumin (Cur) and NDNB.

Methods: We successfully prepared and optimized Cur-loaded chitosan nanoparticles (Cur/CS-VES NPs) and NDNB-loaded chitosan nanoparticles (NDNB/CS-PGA NPs) through a standardized process. In vitro, Calu-3 and HFL1 cells were treated to evaluate the biocompatibility of chitosan nanocarrier materials and the antifibrotic activity of drug-loaded nanoparticles, respectively. In vivo, the bleomycin-induced rat models of pulmonary fibrosis were established to study the efficacy of chitosan nanoparticles.

Results: In vitro experiments indicated that the drug-loaded chitosan nanoparticles exhibited good stability and low cytotoxicity. In vivo pharmacodynamic studies revealed that, compared with oral administration of Cur or NDNB alone, the pulmonary delivery of Cur/CS-VES NPs and NDNB/CS-PGA NPs effectively inhibited the progression of pulmonary fibrosis, improved lung function, reduced levels of inflammatory factors, and mitigated pathological lesions in the lungs. These findings suggest that chitosan-based nano-particles have promising potential as pulmonary inhalation agents for the treatment of pulmonary fibrosis.

Conclusion: These findings highlight the great potential of chitosan-based nanoparticles as a therapeutic strategy for treating IPF and related pulmonary fibrosis with pulmonary delivery pathways.

Keywords: pulmonary drug delivery, nanoparticles, chitosan, idiopathic pulmonary fibrosis, curcumin, nintedanib

Introduction

Pulmonary fibrosis is a chronic and progressive lung disease characterized by the development of fibrous tissue in the lungs, resulting in impaired lung function and respiratory distress.[1] Idiopathic pulmonary fibrosis (IPF) is the most common form of the disease, primarily affecting elderly individuals and associated with a poor prognosis, with a median survival of only 3–5 years.[2–6] The precise cause of IPF remains unknown, but it is believed to involve abnormal proliferation of fibrous tissue and tissue remodeling caused by dysfunctional alveolar epithelial cells and mesenchymal fibroblasts.[7] Additionally, signaling pathways involving tyrosine kinases such as vascular endothelial growth factor (VEGF), fibroblast growth factor (FGF), and platelet-derived growth factor (PDGF) have been implicated in the pathogenesis of IPF.[8–10]

To address the symptoms and progression of pulmonary fibrosis, various treatment options have been explored, including oxygen therapy, lung transplantation, and pharmacotherapy.[11] Oxygen therapy helps alleviate hypoxia in patients, while lung transplantation remains the primary treatment for advanced cases. Pharmacological interventions have demonstrated significant efficacy in managing pulmonary fibrosis. Approved drugs like pirfenidone and nintedanib (NDNB) have different mechanisms of action but both contribute to slowing the decline in lung function,[12–14] extending patient survival, reducing inflammation, and impeding fibrosis progression. Curcumin (Cur) plays a role in anti-inflammatory, anti-fibrosis, anti-oxidation and anti-tumor. An

Received: 4 March 2025
Accepted: 10 October 2025
Published: 25 October 2025

increasing number of studies indicated that Cur has a positive therapeutic effect in the treatment of various lung diseases such as asthma, acute lung injury, lung cancer, pulmonary fibrosis and so on.[15] Nevertheless, both NDNB and Cur exhibit low oral bioavailability. While NDNB is recommended as a first-line therapy for IPF, it still presents therapeutic limitations and significant adverse side effects.[16] Furthermore, while intraperitoneal administration of Cur demonstrates relatively high bioavailability in comparison to the oral route, its efficacy is nonetheless diminished by rapid hepatic metabolism, and parenteral administration cannot circumvent this outcome.[17]

The oral bioavailability of Cur is notably low. A previous study[18] reported that one hour after oral administration of Cur, its plasma concentration was only 11.1 nmol/L. Another research report stated[19] that 2 hours after intake of Cur-like compounds containing 8g of Cur, the concentration of Cur in serum was 156 nmol/L. This limited bioavailability is likely related to the extremely low solubility issue of Cur. Cur is also prone to chemical degradation at neutral and alkaline pH levels and prone to crystallization at acidic pH. The α, β-unsaturated diketone groups in its structure are susceptible to oxidation and lack permeation-enhancing groups.[20] Additionally, Cur undergoes significant first-pass metabolism in the liver and is metabolized by intestinal flora into glucuronide and sulfate conjugates, whose biological activities are significantly lower than those of Cur. Similarly, NDNB exhibits low oral bioavailability, reported to be less than 5%.[21–23] This is likely due to its poor solubility in the relatively neutral intestinal environment. Poor absorption and low bioavailability significantly impact the pharmacodynamic effects of NDNB in the body. Therefore, there is a need for the development of novel drug delivery system to efficiently convey model drugs to the lung and enhance the efficacy of IPF management.

Chitosan (CS), a derivative of the natural polysaccharide chitin, is a polycationic polysaccharide characterized by its availability, biocompatibility, biodegradability, low toxicity, low immunogenicity, and adhesive properties. It has garnered increasing attention in pharmaceutical and biomedical applications.[24] Owing to the presence of functional amino groups on its molecular surface,[25] CS can engage in electrostatic interactions with negatively charged mucus, and it can adhere to the lung mucosa. Consequently, the use of CS in drug formulations for pulmonary delivery enhances drug adhesion to the lung mucosa, facilitates the control of particle size, and thereby prolongs the retention time of drug preparations in the body.[26] Vitamin E succinate (VES) is a derivative of vitamin E, composed of a hydrophobic domain, a signaling domain and a functional domain. It acts on mitochondria and can exert anti-cancer effects. It has high selectivity for cancer cells and very limited or almost non-toxic toxicity to normal cells. Hydrophobicity is a limitation of its clinical treatment.[27] Polyglutamic acid (γ-PGA) is a non-immunogenic and biodegradable anionic homo-polyamide mainly produced by Gram-positive bacteria. Due to its hydrophilicity, biodegradability and biocompatibility, it has become a suitable drug de-livery material and is often used to improve the dispersion of poorly soluble drugs in water. The nanoparticles formed by its negative charge and positively charged chitosan can form stable drug-carrier complexes.[28]

The objective of the present study is to design and develop chitosan-based nanoparticles for pulmonary delivery, with Cur and NDNB as the model drugs, to achieve better therapeutic effect over oral administration. In addition, the present study also aims to compare the therapeutic effects of Cur and NDNB by conducting thorough in vivo pharmacodynamic studies, and evaluate the potential of Cur as an anti-fibrotic agent for lung fibrosis.

Materials and Methods

Materials

Chitosan (CS, molecular weight: 50,000 Da, deacetylation: 75–85%) was obtained from Sigma-Aldrich (Shanghai, China). Curcumin (Cur, 98%) and Tween-80 was purchased from Sinopharm Chemical Reagent Co., Ltd. (Shanghai, China). Nintedanib (NDNB, 99.8%) was purchased from Cangzhou Enke Pharma-tech Co., Ltd. (Hebei, China). Vitamin E succinate (VES, 98%) was bought from Hangzhou Dingyan Chem Co., Ltd. (Hangzhou, China). γ-polyglutamic acid (PGA, 99%) was obtained from Aladdin Chemicals (Shanghai, China). Bleomycin sulfate was purchased from Macklin Biochemical Co., Ltd. (Shanghai, China). All chemicals used were of analytical grade. Nebulizer (403T) was bought from Jiangsu Yuyue Medical Equipment & Supply Co., Ltd. (Jiangsu, China).

Preparation of Chitosan-Based Nanoparticles

Formulation Optimization of Chitosan Nanoparticles

In order to load two different model drugs (Cur and NDNB), different polymeric excipients were chosen to form nanoparticles together with chitosan, respectively, namely Vitamin E succinate (VES) and γ-polyglutamic acid (PGA). The obtained drug loaded chitosan-based nanoparticles were Cur/CS-VES NPs and NDNB/CS-PGA NPs, respectively. Specifically, the Cur/CS-VES NPs were prepared by the emulsion-solvent evaporation method. Cur and VES were dissolved in acetone at concentrations of 5 mg/mL and 2 mg/mL, respectively, while chitosan (0.5mg/mL) was dissolved in a 0.1% acetic acid solution. Under magnetic stirring at 400 rpm, the Cur and VES solutions were slowly added to the chitosan solution, following a specific volume ratio. The nano-suspension was then obtained by stirring in the dark for 20 minutes. After stirring, the Cur/CS-VES NPs suspension was placed into the rotary evaporator at 40°C for 3 min to remove the acetone. Centrifuge (6000rpm, 12min) to remove the free Cur. The supernatant was taken and sonicated in an ice-water bath for 5 min to obtain Cur/CS-VES NPs. When the mass ratio of chitosan to Cur was held constant, the mass ratio of chitosan to VES was systematically adjusted to 1:0.25, 1:0.5, 1:0.7, 1:1, and 1:1.25, respectively. The formulation was optimized based on the particle size, polydispersity index (PDI), drug loading capacity, and encapsulation efficiency of the nanoparticles. Subsequently, using the optimal mass ratio of chitosan to VES, the mass ratio of chitosan to curcumin was further adjusted to 1:0.125, 1:0.25, 1:0.375, 1:0.5, and 1:0.625, respectively, to finalize the composition of Cur/CS-VES NPs.

In the case of NDNB/CS-PGA NPs, NDNB was dissolved in chitosan solution (0.5 mg/mL). Then the PGA solution (2 mg/mL) was dropped into the above NDNB-CS solution under magnetic agitation (800 rpm, 5 min). After that, the obtained solution was transferred to an ultrafiltration tube (4000 Da) and was centrifuged at 2000 rpm for 20 min to remove the free NDNB for obtaining NDNB/CS-PGA NPs. Under the condition of maintaining a constant mass ratio of chitosan and NDNB, nanoparticles (NPs) were prepared using different mass ratios of chitosan to PGA (1:0.1, 1:0.2, 1:0.4, 1:0.6, 1:0.8, respectively) to determine the optimal ratio. Based on the determined optimal mass ratio of chitosan to PGA, the mass ratio of chitosan to NDNB was further adjusted (1:0.3, 1:0.4, 1:0.5, 1:0.6, 1:0.7, respectively) to prepare NPs and ultimately determine the final formula ratio.

Optimization of Preparation Process of Chitosan Nanoparticles

According to the steps in Formulation Optimization of Chitosan Nanoparticles, the preparation process of drug-loaded chitosan nanoparticles was studied.

For Cur/CS-VES nanoparticles, under the specified conditions of chitosan concentration at 0.5 mg/mL, VES concentration at 2 mg/mL, material ratio (CS: VES) at 1:0.7 (m/m), and curcumin concentration at 5 mg/mL with a CS to curcumin ratio of 0.5:1 (m/m), the following optimization steps were conducted. First, the preparation stirring rate was systematically varied from 100 to 500 rpm in increments of 100 rpm, and the particle size, polydispersity index (PDI), encapsulation efficiency (EE%), and drug loading (DL%) of the nanoparticles were evaluated to identify the optimal stirring rate. Second, the stirring time was adjusted to 10, 20, 40, and 60 min, and the same parameters were measured to determine the optimal stirring duration. Third, ultrasonic power was incrementally increased from 50 to 250 W, while maintaining a constant stirring rate of 400 rpm and stirring time of 20 min, to assess its impact on particle size and PDI and to identify the optimal ultrasonic power. Finally, ultrasonic time was varied from 1 to 8 minutes, again keeping the stirring rate at 400 rpm, stirring time at 20 minutes, and ultrasonic power at 150 W, to determine the optimal ultrasonic duration.

For NDNB/CS-PGA nanoparticles, under the specified conditions of chitosan concentration at 0.5 mg/mL, PGA concentration at 2 mg/mL, material ratio (CS: PGA) at 1:0.4 (m/m), and NDNB to CS ratio of 0.5:1 (m/m), the following optimization steps were conducted. First, the preparation stirring rate was systematically varied from 100 to 1000 rpm (100, 200, 400, 600, 800 and 1000 rpm), and the particle size, polydispersity index (PDI), encapsulation efficiency (EE %), and drug loading (DL%) of the nanoparticles were evaluated to identify the optimal stirring rate. Second, the stirring time was adjusted to 2, 5, 10, 20, and 40 minutes, and the same parameters were measured to determine the optimal stirring duration.

Characterization of Drug-Loaded Chitosan Nanoparticles

Characterization of nanoparticles (Cur/CS-VES and NDNB/CS-PGA) included the determination of particle size, polymer dispersion index (PDI) and ζ potential with Malvern Zetasizer Nano ZS 90 (Worcestershire, UK) and the observation of nanoparticle morphology with transmission electron microscopy (TEM, Hitachi, Japan). The prepared chitosan nanoparticles were stored at 4 °C in the dark. The particle size of the nanoparticles was measured on days 1, 5, 10, and 15 to evaluate the stability of the preparation. The drug entrapment efficiency (EE %) and drug loading (DL %) of the Cur in Cur/CS-VES NPs and the NDNB in NDNB/CS-PGA NPs was determined using ultraviolet spectrophotometry at 420 and 391 nm, respectively. The equations for calculating the EE and DL were as follows:

$$\mathrm{EE}(\%) = \frac{Weight\ of\ API - Weight\ of\ free\ API}{Weight\ of\ API} \times 100\% \quad (1)$$

$$DL(\%) = \frac{Weight\ of\ API - Weight\ of\ free\ API}{Weight\ of\ NPs} \times 100\% \quad (2)$$

In vitro Release and Stability of NPs

Cur/CS-VES NPs and NDNB/CS-PGA NPs were sealed in dialysis bags (MWCO = 4 kDa for Cur and 10 kDa for NDNB). The dialysis bags were immersed into 500mL phosphate buffered saline (PBS, pH 7.4) containing 0.5% (w/v) Tween-80 and stirred (100 rpm, 37°C) for 48 hours. At the present time point, 5 mL of the release solution is collected and the same volume of the release medium is replenished for the detection of drug concentration by HPLC at the wavelength of 420 nm for Cur and 391 nm for NDNB, respectively. In-vitro release experiments were performed three times. The drug-loaded chitosan nanoparticles were stored at 4°C and the stability of nanoparticles was investigated.

In vitro Cytotoxicity Studies

Cytotoxicity

The concentrations ranging from 1.56 to 100 mg/mL of the API (Cur & NDNB) and formulation (Cur/CS-VES & NDNB/CS-PGA NPs) were diluted into the culture medium (MEM) for the evaluation in Calu-3 cells (American Type Culture Collection, ATCC). To be specific, drugs were added and incubated with the cells for 48h after the Calu-3 cells cultured for 24 h in 96-well plates (1×10^4 cells/well). MTT solution (5 mg/mL) was added to for another 4 h (20 μL/well). After that, the supernatant was discarded, 200 μL dimethyl sulfoxide (DMSO) was added to each well with 5–10 min shaking to dissolve the formazan crystals. The OD value of each well was recorded by a microplate reader (BioTek, USA) at 490 nm.

Inhibition of HFL1 Growth

Human fetal lung fibroblast 1 (HFL1) was applied to evaluate the anti-fibrosis effect of the nanoparticles and was purchased from ATCC. After 24 hours of culturing HFL1 cells in 96-well plates (1×10^4 cells/well), the diluted solutions of API and nanoparticles (1.56 to 100 mg/mL) were added to the well for 48-hour incubation. Subsequently, 20 μL MTT solution (5 mg/mL) was added to each well for 4 h. The supernatant was removed and 200 μL DMSO was added to each well with 5–10 min shaking. Finally, the results were obtained at 490 nm by a microplate reader.

In vivo Pharmacodynamic Study

Grouping and Administration

The pulmonary fibrotic rat model induced by bleomycin (BLM; concentration: 4 mg/mL; dose: 5 mg/kg,) was established via intratracheal administration.[29] Specifically, the male SD rats (6 weeks) were divided randomly into 5 groups: (i) blank (n=5); (ii) model (n=5); (iii) oral API (30 mg/kg for Cur, 10 mg/kg for NDNB, n=5+5); (iv) inhaled API (5 mg/kg for Cur, 3 mg/kg for NDNB, n=5+5); (v) inhaled NPs (5 mg/kg for Cur, 3mg/kg for NDNB, n=5+5); After modeling, the rats in the inhaled group were put into a cubic cage, which was connected with an ultrasonic nebulizer. And the rats in the oral group were administrated via a gavage needle. Twenty-eight days post-treatment, the lungs of the rats were harvested to determine the lung function, lung coefficient, histopathology changes (H&E and Masson), cytokines (TGF-β1 and IL-6) and biomarkers (SOD, Hyp). All animal experiments received approval from and were conducted under the supervision of the laboratory animals ethical committee of

Zhejiang University of Technology (Approval No. MGS20220908079) and use of Laboratory Animals (Approval No. MGS20220908079) and the National In-stitutes of Health Guide for Care and Use of Laboratory Animals (Publication No. 85–23, revised 1996). Humane care was ensured for the animals throughout the experimental process.

Measurement of Lung Function

The small animal lung function tester (WBP, Shanghai Tawang Intelligent Technology Co., Ltd.) was applied to investigate the diverse respiratory indicators in rats on day 28, including the inspiratory time (TI), the respiratory rate (RR), the expiratory time (TE), the tidal volume (VT), the peak expiratory flow (PEF), the peak inspiratory flow (PIF), the inspiratory-to-expiratory ratio (Volbal, TI: TE), the mid-expiratory tidal flow (EF50, expiratory flow rate at 50% of expiratory volume), etc.

Lung Coefficient Measurement

The weights of all rats were recorded daily throughout the experiment. After 28 days of continuous administration, the weight of wet lungs in each group was measured for the calculation of lung coefficient (Eq.3). Typically, a high lung coefficient implies the significant inflammation and fibrosis.

Measurement of TGF-β1 and IL-6 in BALFs

The bronchoalveolar lavage fluids (BALFs) were collected from the left lung by washing three times with saline. Then BALF samples were centrifuged at 3500 rpm for 10 min (4 °C), which were subjected to ELISA for determination of inflammatory factor content: transforming growth factor-β1 (TGF-β1) and interleukin-6 (IL-6). The corresponding ELISA kits for the TGF-β1 and IL-6 (Wuhan Boster Biological Technology., Ltd, China) were employed, and the optical density was recorded on a microplate reader at 450 nm.

Measurement of Hyp and SOD in the Lung Tissue

The tissue of left lung was washed with physiological saline and dried with filter paper. Homogenized in the ice-water bath and centrifuged for 10 min (4000rpm, 4°C). The supernatant was taken out to measure the content of hydroxyproline (Hyp) and superoxide dismutase (SOD) in the lung tissue via the corresponding assay kits (Nanjing Jiancheng Biotechnology Engineering Research Institute, China).

Histopathological Analysis

The right lung tissue was dried using filter paper and then fixed in 4% paraformaldehyde for 24 h, which was sent to Wuhan Boster Biological Technology., LTD for Hematoxylin and Eosin (H&E) staining and Masson's Trichrome staining for obtaining 5 μm thick slices.

Statistical Analysis

Statistical analyses and calculations were conducted on GraphPad Prism 9.0 (Dotmatics, USA). Each batch was repeated three times and the results were expressed as mean ± standard deviation (SD). One-way analysis of variance (ANOVA) was employed for the statistical analysis, with $p<0.05$ and $p<0.01$ representing statistically significant.

Results and Discussion

Optimization and Characterization of Drug-Loaded CS Nanoparticles

Chitosan nanoparticles were firstly characterized and optimized to allow a uniform particle distribution, high drug loading rate and high entrapment efficiency. For the Cur/CS-VES nanoparticles (Figure 1aI–IV), when the material ratio of CS to VES was 1:0.7, we achieved the highest EE (%) of 60.1±2.9% and DL (%) of 11.7±0.5%. This ratio also showed the smallest particle size of 307.4±7.5 nm and a PDI of 0.233±0.068. By adjusting the carrier-to-drug ratio (chitosan to curcumin) to 1:0.5, the optimal conditions were slightly altered, yielding a final EE (%) of 56.61±1.77%, DL (%) of 14.27 ±0.38%, particle size of 301.2±4.3 nm, and a PDI of 0.266±0.078.

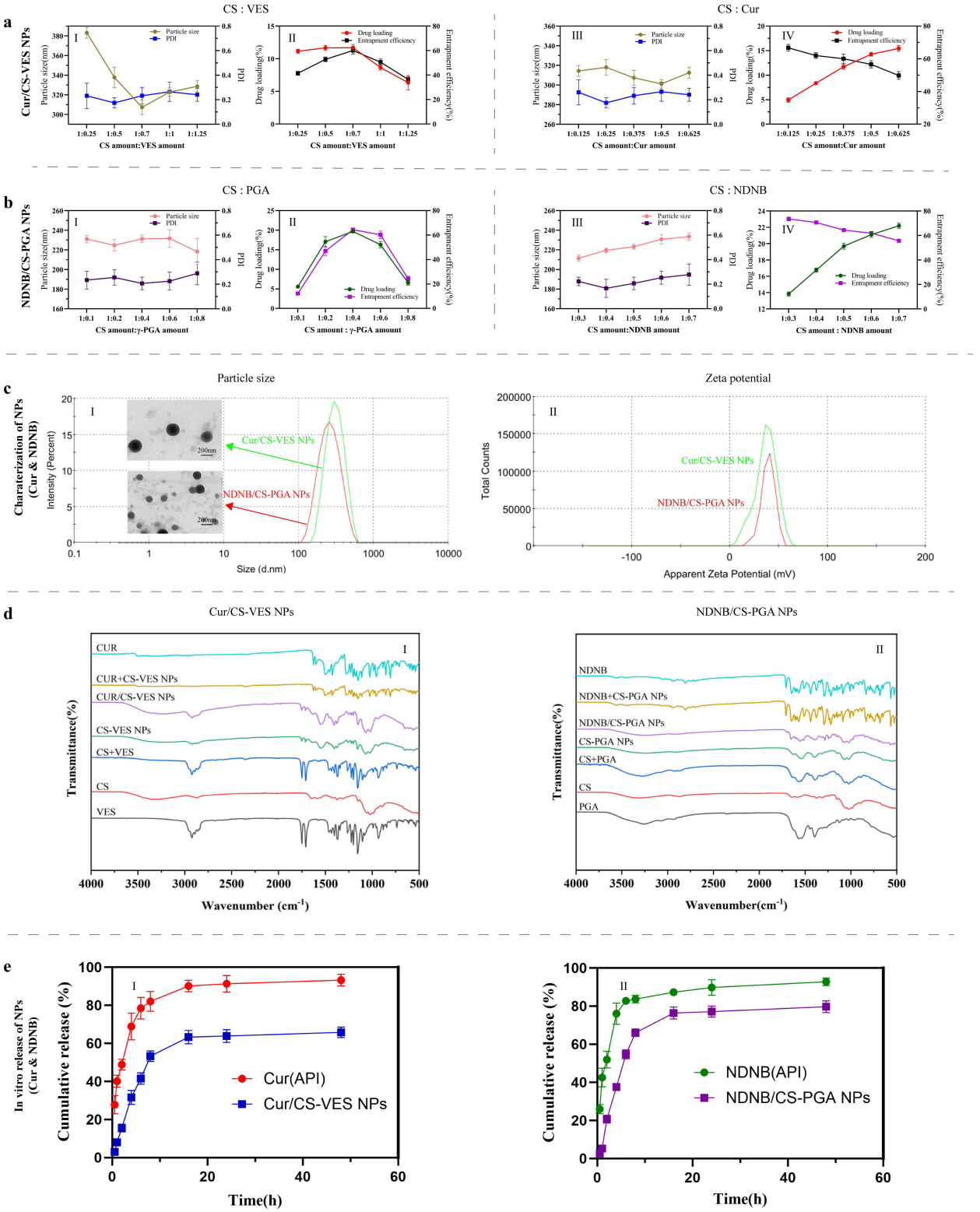

Figure 1 The optimization and characterization of drug-loaded chitosan nanoparticles: for Cur/CS-VES NPs, the effects of material ratio on particle size and PDI (**a**-I) and EE & DL (**a**-II), the effects of carrier to drug ratio on particle size and PDI (**a**-III) and EE & DL (**a**-IV); similarly, the optimization of NDNB/CS-PGA NPs (**b** I-IV); the particle size (**c**-I) and zeta potential (**c**-II) of optimized NPs (Green for Cur/CS-VES, Red for NDNB/CS-PGA); the IR graph of NPs (d-I for Cur/CS-VES NPs, d-II for NDNB/CS-PGA NPs); the in-vitro release of NPs (**e**-I for Cur/CS-VES NPs, e-II for NDNB/CS-PGA NPs, n=3). The results represent the mean ± SD.

For the NDNB/CS-PGA nanoparticles (Figure 1bI–IV), the optimal conditions were explored using a material ratio of CS to PGA of 1:0.4 and a carrier-to-drug ratio of CS to NDNB of 1:0.5. Under these conditions, we attained an EE (%) of 67.03 ± 0.45%, DL (%) of 19.70 ± 0.14%, a minimal particle size of 223.3 ± 2.5 nm, and a PDI of 0.207 ± 0.051.

Based on the optimization results of the preparation process (Tables S1–S6), the optimal parameters for preparing Cur/CS-VES NPs were determined as follows: a stirring rate of 400 rpm, a stirring duration of 20 min, an ultrasonic power of 150 w, and an ultrasonic treatment time of 4 min. For the preparation of NDNB/CS-PGA NPs, the optimal stirring rate was 800 rpm and the optimal stirring duration was 5 min.

The particle size stability of the nanoparticles is presented in Table 1. According to the data in the table, the particle size of the nanoparticles exhibits a gradual increase over time, which may be attributed to the formation of a hydration layer due to the interaction between the nanoparticle's outer layer and water molecules. Within the first 15 days, the particle size of the drug-loaded nanoparticles remains relatively constant, indicating excellent stability. TEM, distribution of particle size, and zeta potential analysis were applied to fully characterize the optimized Cur and NDNB nanoparticles. As shown in Figure 1cI–II, the Cur/CS-VES nanoparticles exhibited a spherical morphology with a single peak at 314.0 nm in size distribution, indicating uniformity, and a high zeta potential of +36.6 mV. Similarly, the NDNB/CS-PGA nanoparticles demonstrated a smaller particle size, peaking at 267.9 nm, along with a higher zeta potential of +39.6 mV when compared to the Cur/CS-VES nanoparticles. These characteristics suggest that the positively charged chitosan significantly enhances the stability of the drug-loaded chitosan nanoparticles. Figure 1d-I shows the physical mixture of CUR, CUR and CS-VES nanoparticles (CUR+CS-VES NPs), CS-VES blank nanoparticles (CS-VES NPs), and CUR/CS-VES FT-IR map analysis of NPs. In the physical mixture of CS and VES, it is manifested as a simple superposition of the characteristic peaks of CS and VES, without obvious new peaks or peak position shifts, indicating that no significant chemical interaction occurs between the two in the physical mixture state. In CS-VES NPs, the 1709 cm^{-1} of VES -COOH weakened, presenting a new peak of $-COO^-$ with asymmetric stretching vibration of 1557 cm^{-1} and a new peak of symmetrical vibration of 1405 cm^{-1}. The 1591 cm^{-1} peak of chitosan $-NH_2$ weakened. The enhancement of the $-NH_3+$ peak at 1557 cm^{-1} indicates that the amino group of chitosan forms an electrostatic complex with the $-COO^-$ of VES. In the physical mixture of CUR and CS-VES NPs, it is manifested as a simple superposition of the characteristic peaks of CUR and CS-VES NPs, without obvious new peaks or peak position shifts, indicating that no significant chemical interaction occurs between the two in the physical mixture state. However, in CUR/CS-VES NPs, the characteristic absorption peak of CUR is masked or weakened, but the characteristic peak of CS-VES NPs still exists, indicating that the drug may have been successfully encapsulated. Figure 1d-II shows the physical mixture of NDNB, NDNB and CS-PGA blank nanoparticles (NDNB+CS-PGA NPs), CS-PGA blank nanoparticles (CS-PGA NPs), and NDNB nanoparticles (NDNB/CS-PGA) FT-IR map analysis of NPs. In the physical mixture of CS and PGA, it is manifested as a simple superposition of the characteristic peaks of CS and PGA, without obvious new peaks or peak position shifts, indicating that in the physical mixture state, there is no significant chemical interaction between CS and PGA. Furthermore, the amino peak of chitosan in CS-PGA NPs weakened, the $-NH_3+$ at 1540 cm^{-1} increased, and the $-COO^-$ peak of PGA shifted red from 3255 cm^{-1} to 3243 cm^{-1}, and merged into a single wide peak. Indicating electrostatic recombination with $-COO^-$ of PGA, the amide II band of PGA redshifts to 1540 cm^{-1}, and the asymmetric stretching vibration (ν_{as} COO^-) redshifts from 1574 cm^{-1} to 1540 cm^{-1}, further demonstrating the electrostatic interaction. In the physical mixture of NDNB and CS-PGA NPs, it is manifested as a simple superposition of the characteristic peaks of NDNB and CS-PGA NPs, without obvious new peaks or peak position shifts, indicating that no significant chemical interaction occurs between the two in the physical mixture state. However, in NDNB/CS-PGA NPs, the characteristic absorption peaks of NDNB were masked or weakened, but the characteristic peaks of CS-PGA NPs still existed, indicating that the

Table 1 The Particle Size Stability of Drug-Loaded Nanoparticles (n=3)

NPs/Time (d)	1	5	10	15
Cur/CS-VES NPs	361.1±5.07 nm	384.2±6.2 nm	391.3±6.4 nm	402.5±5.3 nm
NDNB/CS-PGA NPs	223.3±2.49 nm	232.5±4.3 nm	246.2±5.3 nm	263.3±7.5 nm

https://doi.org/10.2147/IJN.S522929

drug might have been successfully encapsulated. The results of the drug release experiment demonstrated that Cur/CS-VES NPs released Cur at a slower over the plain drug (Cur) (Figure 1e-I), indicating that Cur/CS-VES NPs could achieve a sustained release behavior. A similar specificity was observed for NDNB/CS-PGA NPs (Figure 1e-II).

Biocompatibility and in vitro Studies

The cytotoxicity of API (Cur & NDNB) and NPs (Cur/CS-VES & NDNB/CS-PGA) was co-cultured with Calu-3 and HFL1 cells by the MTT assay. With the increase of NPs concentration from 1.56 to 100 μg/mL, all cell viabilities were above 80%, demonstrating that all carrier materials are biocompatible with Calu-3 cells (Figure 2a-I and b-I). In addition, IC50 (half maximal inhibitory concentration) of the NPs were obviously higher than that of API for both Cur (31.64 vs 25.44 μg/mL) and NDNB (48.75 vs 35.00 μg/mL). This suggests that the drug-loaded nanoparticles exhibit lower cytotoxicity compared to the pure APIs.

After confirming the biocompatibility, the in vitro anti-fibrosis activity of API and drug-loaded nanoparticles was further studied on HFL1 cells (Figure 2a a-II and b-II). Specifically, the inhibition rate of drug to HFL1 was dose-dependent, suggesting the favorable anti-fibrosis effect. Moreover, the drug-loaded NPs groups exhibited distinctly lower IC50 (Cur: 14.89 vs 23.86 μg/mL; NDNB: 12.53 vs 17.84 μg/mL) compared to the free drug groups, with Cur showing IC50 values of 14.89 μg/mL versus 23.86 μg/mL and NDNB showing values of 12.53 μg/mL versus 17.84 μg/mL. These findings reveal that formulating the drugs into CS NPs enhances their anti-fibrosis effects.

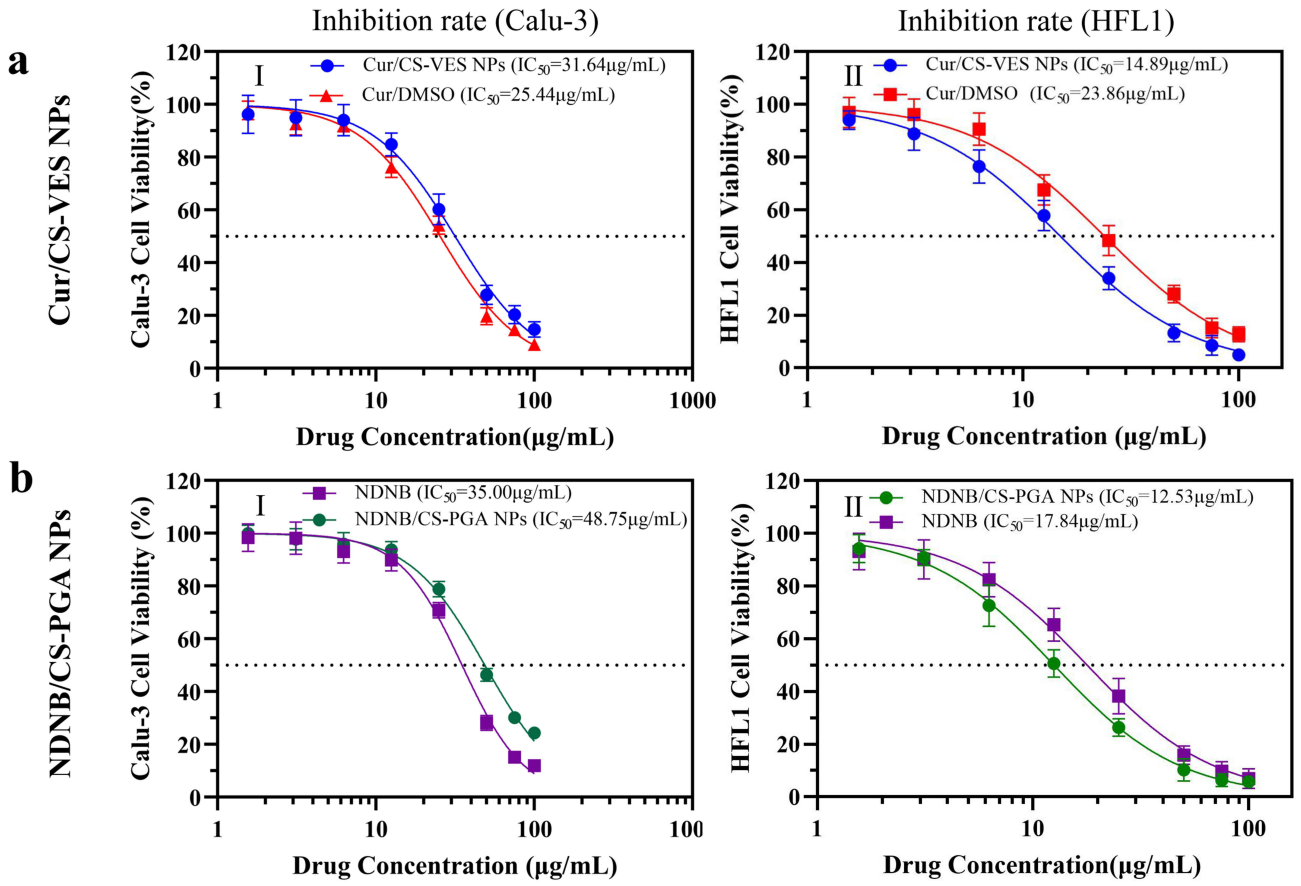

Figure 2 Inhibition rate of Cur and Cur/CS-VES NPs on Calu-3 (**a**-I) and HFL1 (**a**-II); similarly, inhibition rate of NDNB and NDNB/CS-PGA NPs (**b** I-II) (n=5). The results represent the mean ± SD.

In vivo Pharmacodynamics

Lung Function

Test of lung function is a crucial clinical examination for assessing respiratory diseases, as it indicates the severity of lung conditions and changes in lung pathophysiology.[30] The corresponding lung function parameters are illustrated in Figure 3. In contrast, the API (oral), API (inhalation), NPs groups (inhalation) all showed improved lung function parameters, with higher TI, TE, and TV values compared to the model group. The inhaled NPs group demonstrated superior RR, TI, TE, VT, PIF, PEF, and EF50 parameters compared to the API groups. Among the treatment groups, the respiratory rates decreased in the order of API (oral), API (inhalation) and NPs (inhalation). As a consequence of the elevated respiratory rate, inspiratory time, expiratory time, and volume per breath were shortened. Additionally, the volume of tidal breaths decreased due to the reduced lung elasticity caused by pulmonary fibrosis, while peak inspiratory flow, peak expiratory flow, and expiratory flow at 50% of forced vital capacity (EF50) increased. These findings suggest that the nebulized administration of chitosan nanoparticles containing Cur or NDNB can both significantly improve lung function indices in rats with pulmonary fibrosis.

Lung Coefficient

The lung coefficient is a crucial indicator of pulmonary edema, reflecting the severity of pulmonary fibrosis. It is calculated using Equation 3, with rat weight provided in Figure 4a-I, b-I. Following the administration of BLM, there was a significant decrease in body weight among the rats compared to the blank group. However, in the treated group, the rate of decline in body weight was relatively slower after 5 days of administration. Notably, in the inhaled NPs groups, there was a reversal of this trend, with body weight beginning to increase on the fifth day. This suggests a potential therapeutic effect of the NPs in alleviating the adverse impacts of BLM on body weight.

The results of the lung coefficients for each group are illustrated in Figure 4a-II and b-II. The model group exhibited the highest lung coefficient, while the blank group ranked the lowest ($P < 0.001$). Administration of APIs (Cur and NDNB) via gavage and inhalation reduced lung coefficients in bleomycin (BLM) model rats. Notably, the inhaled nanoparticle (NP) treatment further decreased lung coefficients in these rats. The APIs proved effective against pulmonary fibrosis, with the most significant improvement observed in the inhaled NPs groups (Cur/CS-VES NPs and NDNB/CS-PGA NPs), which showed a significant difference ($P < 0.001$) compared to the blank group. This suggests that inhaled NPs are particularly effective in alleviating pulmonary fibrosis. The limited efficacy of the API in alleviating

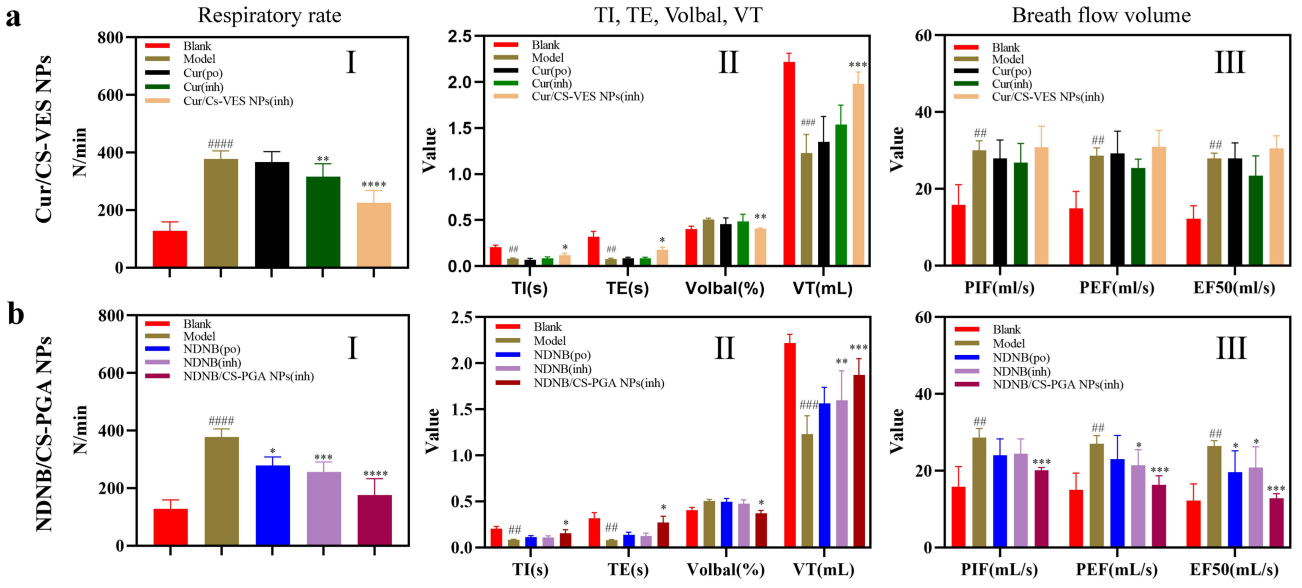

Figure 3 The respiratory rate (**a-I, b-I**); the inspiratory time (TI), the expiratory time (TE), the inspiratory-to-expiratory ratio (Volbal, TI: TE) and the tidal volume (VT) (**a-II, b-II**); the breath flow volume (The peak expiratory flow, PEF; The peak inspiratory flow, PIF; The mid-expiratory tidal flow, EF50) (**a-III, b-III**) for Cur/CS-VES NPs and NDNB/CS-PGA NPs ordered by blank, model, oral API (po), inhaled API (inh) and inhaled NPs (inh). The results represent the mean ± SD. $^{\#\#}p < 0.01$, $^{\#\#\#\#}p < 0.001$, $^{\#\#\#\#\#}p < 0.0001$ versus the blank group; $^{*}p < 0.05$, $^{**}p < 0.01$, $^{***}p < 0.001$, $^{****}p < 0.0001$ versus the model group.

https://doi.org/10.2147/IJN.S522929

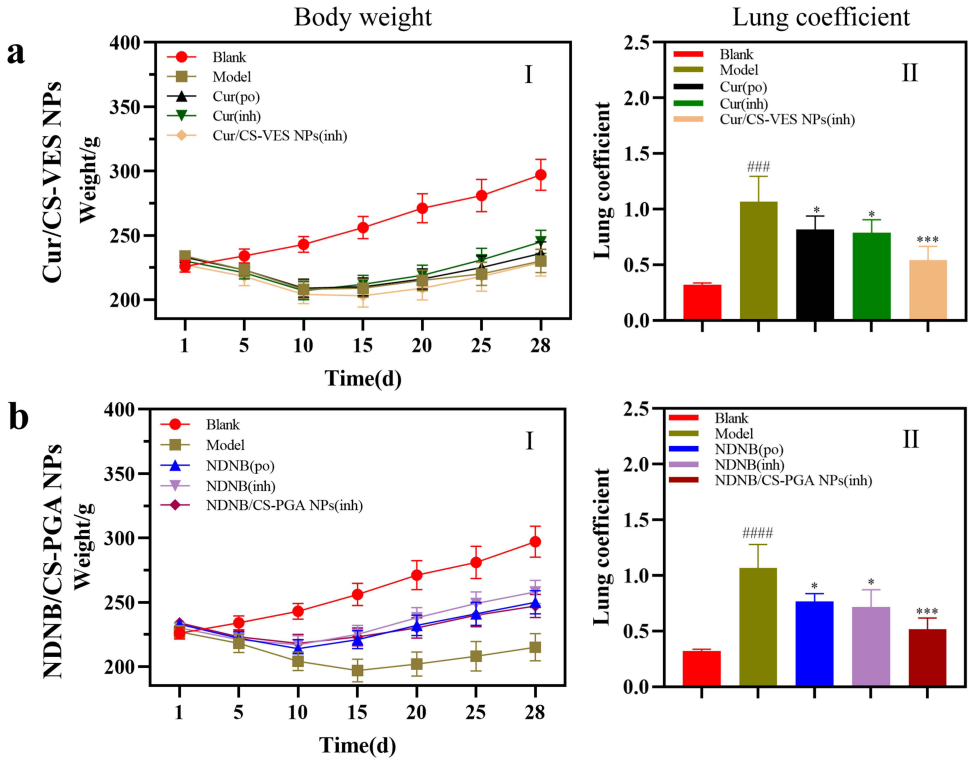

Figure 4 The body weight (**a**-I) and lung coefficient (**a**-II) in the Cur group ordered by blank, model, oral API (Cur, po), inhaled API (Cur, inh) and inhaled NPs (Cur/CS-VES NPs, inh). Similarly, the body weight (**b**-I) and lung coefficient (**b**-II) in the NDNB group ordered by blank, model, oral API (NVNB, po), inhaled API (NDNB, inh) and inhaled NPs (NDNB/CS-PGA NPs, inh). ###p < 0.001, #####p < 0.0001 versus the blank group; *p < 0.05, ***p < 0.001 versus the model group. The results represent the mean ± SD, n=5.

pulmonary edema may be attributed to its inadequate absorption and low bioavailability in vivo.[31,32] Conversely, the NPs groups may achieve an appropriate blood concentration, effectively reducing the lung coefficient.

Biomarkers: TGF-β1, IL-6, Hyp, SOD

In the presence of lung damage, high levels of TGF-β1 generated by immune cells during inflammation led to fibrosis of the organ.[33,34] Excessive TGF-β1 levels contribute to the fibrosis and remodeling of the lungs through stimulating myofibroblasts to produce proteins of collagen and extracellular matrix. TGF-β1 gives a promotion to fibroblasts in proliferation and transformation and induces tissue fibrosis by endothelial mesenchymal transition. It also triggers the conversion of epithelial cells and fibroblasts into myofibroblasts.[35] Interstitial lung disease shows the elevation of pro-fibrotic/pro-inflammatory cytokines such as interleukin IL-6, amplifying the fibrotic process.

Oxidative stress (OS) plays a crucial role in the pathogenesis of pulmonary fibrosis. It leads to damage and necrosis of alveolar epithelial cells, apoptosis of lung epithelial cells, and promotes epithelial-mesenchymal transition.[36] Superoxide dismutase (SOD) is an indicator of OS, reflecting both the damage of reactive oxygen species to cells during pulmonary dysfunction and the ability of the body to scavenge oxidative free radicals.[37]

Hydroxyproline (Hyp) is primarily found in collagen, and the amount of Hyp in lung tissue correlates with collagen levels.[30] An elevation in Hyp content signifies abnormal accumulation of extracellular matrix components and inflammatory symptoms within the pulmonary tissue. BLM contributes to these effects when it induces OS in rat lung tissue. Overall, these factors, including TGF-β1, IL-6, SOD and Hyp content, play crucial roles in the pathogenesis and progression of pulmonary fibrosis.

To figure out whether APIs and NPs could put off the progression of lung fibrosis by attenuating the inflammatory factors and marker expression of lung fibroblast, the performance of TGF-β1, IL-6, Hyp and SOD in lung tissues were assayed (Figures 5 and 6). The TGF-β1/Smad3 pathway is the key signal pathway in a rat model of pulmonary fibrosis.[38] Factors of TGF-β1 and IL-6 could be released on account of facilitation by BLM (Figure 5), while APIs and NPs

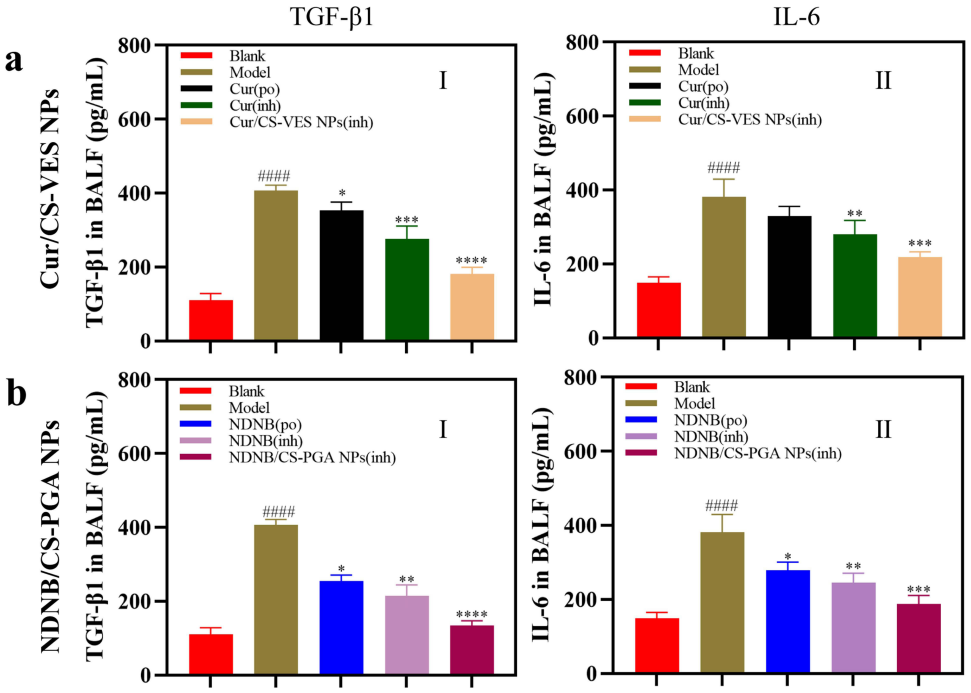

Figure 5 The TGF-β1 expression (a-I) and IL-6 expression (a-II) in BALF for Cur administration group (ordered by blank, model, oral API, inhaled API and inhaled NPs, n=5). Similarly, the biomarkers in NDNB group (b I-II). ####p < 0.0001 versus the blank group; *p < 0.05, **p < 0.01, ***p < 0.001, ****p < 0.0001 versus the model group. The results represent the mean ± SD.

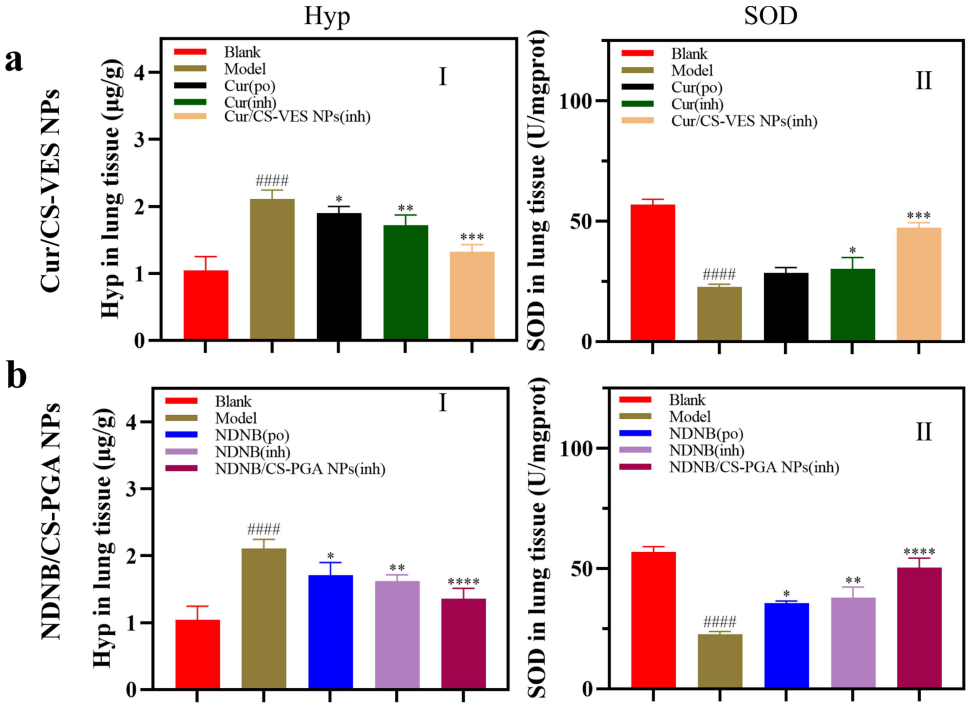

Figure 6 The level of Hyp (**a-**I) and SOD (**a-**II) in lung tissue for Cur administration group (ordered by blank, model, oral API, inhaled API and inhaled NPs, n=5). Similarly, the biomarkers in NDNB group (**b** I-II). ####p < 0.0001 versus the blank group; *p < 0.05, **p < 0.01, ***p < 0.001, ****p < 0.0001 versus the model group. The results represent the mean ± SD.

https://doi.org/10.2147/IJN.S522929

inhibited this process to various degrees. In addition, in the study of inhibiting pulmonary fibrosis in rats, inhaled NPs ($P<0.001$) had the best therapeutic effect, followed by inhaled APIs ($P<0.01$), and oral APIs ($P<0.05$).

Regarding Hyp levels in lung tissue (Figure 6a-I, b-I), they were significantly elevated after the induction of pulmonary fibrosis by bleomycin ($P<0.0001$) and decreased after administration, particularly in the NPs group, where the decrease was most pronounced. In the case of SOD (Figure 6a-II, b-II), its content decreased after the administration of bleomycin ($P<0.0001$) and increased after subsequent treatments. The increase in SOD content followed the order of inhalation administration of NPs (inhaled), API (inhaled), and API (gavage).

These findings demonstrated that Cur and NDNB increased the antagonistic effects of BLM on fibroblasts and prevented the TGF- β signaling pathway from being activated. By decreasing collagen deposition, lowering the inflammatory response, and inhibiting lung fibroblast proliferation, Cur and NDNB effectively stopped the advancement of pulmonary fibrosis. Rats with BLM-induced lung fibrosis have shown a possible therapeutic benefit by Cur and NDNB. However, the exact mechanism underlying this action is still unknown.

Histopathology (H&E, Masson)

The effect of APIs and NPs therapy on lung tissue in rats with pulmonary fibrosis was displayed in Figures 7 and 8. In Figure 7, the H&E-stained lung sections from the blank group exhibited normal lung architecture, characterized by thin alveolar walls, clear contours, normal-sized alveoli, and rounded nuclei of alveolar epithelial cells and no signs of necrosis were observed. The pulmonary fibrosis model was successfully built by BLM (5 mg/kg). BLM-treated rats displayed severe structural abnormalities, including incomplete alveolar structures, inflated alveoli, and thickened alveolar walls. Focal hemorrhages were also observed in the field of view, with a prominent presence of red blood cells, as well as dense inflammatory infiltrates and significant pigmentation. Treatment with APIs (Cur and NDNB) alleviated most of the histopathological lesions induced by BLM. Inhaled API administration resulted in partial recovery of alveolar structures; however, some alveolar wall thickening and mild alveolar epithelial cell hyperplasia persisted. Upon the formation of chitosan nanoparticles, the NPs further improved the restoration of the alveolar structure. This was evident by thinner alveolar walls, reduced tissue hemorrhage, and decreased inflammatory infiltration. Although a few

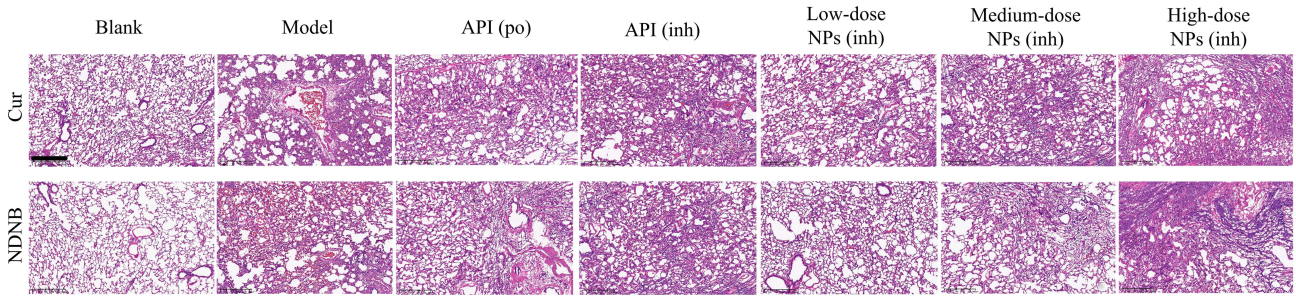

Figure 7 H&E staining of lung tissue in the Cur and NDNB group (ordered by blank, model, oral API, inhaled API and inhaled NPs), scale bar represents 400 μm.

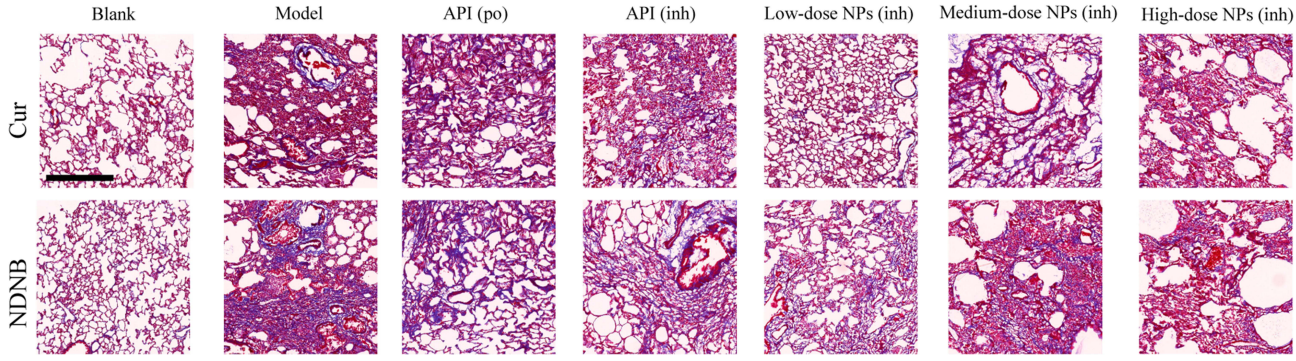

Figure 8 Masson staining of lung tissue in the Cur and NDNB group (ordered by blank, model, oral API, inhaled API and inhaled NPs), scale bar represents 400 μm.

red blood cells were still visible, the overall improvement was notable The effectiveness of alveolar structure restoration varied among the different treatment groups.

The inhaled NPs group has the best treatment effect, with the analysis of the lung structure in this group revealed similarities to that of the blank group, followed by the inhaled API, and gavage API groups, respectively (Figure 7). The degree of damage to bronchial epithelial cells was diminished, which decreased the conversion of epithelial cells to mesenchymal cells.

The Masson's trichrome-stained lung sections from the blank group exhibited minimal deposition of collagen fibers around the bronchioles and blood vessels (Figure 8). In contrast, rats treated with BLM displayed a significant increase in collagen fibers deposition, accompanied by severe bleeding. The deposition of collagen fibers was observed to be concentrated around the walls of alveoli, bronchioles, and blood vessels. Treatment with APIs (Cur and NDNB) resulted in a reduction in collagen fibers deposition around the blood vessels and bronchioles compared to the BLM-treated rats. Additionally, there was a decrease in hemorrhage. Moreover, the deposition of collagen fibrils and the extent of hemorrhage were more prominently reduced in the groups receiving inhaled administration of NPs compared to the groups receiving APIs administration (Figure 8).

These findings suggest that the treatment with APIs, particularly when delivered through inhalation in the form of chitosan nanoparticles, effectively mitigated the deposition of collagen fibers and reduced hemorrhage in the lung tissues of BLM-treated rats. This indicates the potential therapeutic benefits of the inhaled NPs in reducing fibrosis and tissue damage associated with bleomycin-induced lung injury.

Conclusions

Pulmonary fibrosis is a severe and often fatal disease with an unclear underlying mechanism, though it is known to involve inflammation and transformation of fibroblasts into myofibroblasts, induced by TGF-β1. In this study, chitosan-based nanoparticles (Cur/CS-VES and NDNB/CS-PGA) were designed and developed to effectively deliver drugs (curcumin/-nintedanib) to the affected lung tissue for the treatment of pulmonary fibrosis rats. The results suggested that these Cur/CS-VES and NDNB/CS-PGA nanoparticles significantly delayed the decline in lung function parameters, reduced inflammation and cytokine levels, alleviated pathological lung lesions, and improved the bioavailability and antifibrotic effectiveness of the drugs in pulmonary fibrosis rats. These findings highlight the significant potential of chitosan-based inhalation nanoparticles as a therapeutic strategy for treating pulmonary fibrosis and associated pulmonary fibrosis.

Acknowledgments

This research was funded by the National Natural Science Foundation of China (No. 22078297, 22478355), Natural Science Foundation of Zhejiang Province (LY19B060012, LY20B060007) and Zhejiang Provincial Traditional Chinese Medicine Science and Technology Project (2025ZL027).

Disclosure

The authors report no conflicts of interest in this work.

References

1. Raghu G, Collard HR, Egan JJ, et al. An official ATS/ERS/JRS/ALAT statement: idiopathic pulmonary fibrosis: evidence-based guidelines for diagnosis and management. *Am J Respir Crit Care Med*. 2011;183:788–824. doi:10.1164/rccm.2009-040GL
2. Nicholson AC, Colby TV, Dubois RM, Hansell DM, Wells AU. The prognostic significance of the histologic pattern of interstitial pneumonia in patients presenting with the clinical entity of cryptogenic fibrosing alveolitis. *Am J Respir Crit Care Med*. 2000;162:2213–2217. doi:10.1164/ajrccm.162.6.2003049
3. Olson AL, Swigris JJ, Lezotte DC, Norris JM, Wilson CG, Brown KK. Mortality from pulmonary fibrosis increased in the United States from 1992 to 2003. *Am J Respir Crit Care Med*. 2007;176:277–284. doi:10.1164/rccm.200701-044OC
4. Yang XB, Yu Y, Xu JQ, et al. Clinical course and outcomes of critically ill patients with SARS-CoV-2 pneumonia in Wuhan, China: a single-centered, retrospective, observational study. *Lancet Respir Med*. 2020;8:475–481. doi:10.1016/S2213-2600(20)30079-5
5. Nakahira K, Cloonan SM, Mizumura K, Choi AMK, Ryter SW. Autophagy: a crucial moderator of redox balance, inflammation, and apoptosis in lung disease. *Antioxid Redox Signal*. 2014;20:474–494. doi:10.1089/ars.2013.5373
6. Ma J, Li G, Wang H, Mo CH. Comprehensive review of potential drugs with anti-pulmonary fibrosis properties. *Biomed Pharmacother*. 2024;173:116282. doi:10.1016/j.biopha.2024.116282

7. Selman M, King TE, Pardo A. Idiopathic pulmonary fibrosis: prevailing and evolving hypotheses about its pathogenesis and implications for therapy. *Ann Intern Med*. 2001;134:136–151. doi:10.7326/0003-4819-134-2-200101160-00015
8. Chaudhary NI, Roth GJ, Hilberg F, et al. Inhibition of PDGF, VEGF and FGF signalling attenuates fibrosis. *Eur Respir J*. 2007;29:976–985. doi:10.1183/09031936.00152106
9. Wolters PJ, Collard HR, Jones KD. Pathogenesis of idiopathic pulmonary fibrosis. *Annu Rev Pathol*. 2014;9:157–179. doi:10.1146/annurev-pathol-012513-104706
10. Abbas NAT, Nafea OE, Mohammed HO, et al. Repurposing of carvedilol to alleviate bleomycin-induced lung fibrosis in rats: repressing of TGF-β1/α-SMA/Smad2/3 and STAT3 gene expressions. *Life Sci*. 2023;324:121692. doi:10.1016/j.lfs.2023.121692
11. Laporta Hernandez R, Aguilar Perez M, Lázaro Carrasco MT, Ussetti Gil P. Lung transplantation in idiopathic pulmonary fibrosis. *Med Sci*. 2018;6:68. doi:10.3390/medsci6030068
12. Richeldi L, du Bois RM, Raghu G, et al. Efficacy and safety of nintedanib in idiopathic pulmonary fibrosis. *N Engl J Med*. 2014;370:2071–2082. doi:10.1056/NEJMoa1402584
13. King TE Jr, Bradford WZ, Castro-Bernardini S, et al. A Phase 3 trial of pirfenidone in patients with idiopathic pulmonary fibrosis. *N Engl J Med*. 2014;370:2083–2092. doi:10.1056/NEJMoa1402582
14. Selvarajah B, Platé M, Chambers RC. Pulmonary fibrosis: emerging diagnostic and therapeutic strategies. *Mol Aspects Med*. 2023;94:101227. doi:10.1016/j.mam.2023.101227
15. Pulido-Moran M, Moreno-Fernandez J, Ramirez-Tortosa C, Ramirez-Tortosa MC. Curcumin and Health. *Molecules*. 2016;21:264. doi:10.3390/molecules21030264
16. Kaur R, Shaikh TB, Sripadi HP, et al. Nintedanib solid lipid nanoparticles improve oral bioavailability and ameliorate pulmonary fibrosis in vitro and in vivo models. *Int J Pharm*. 2024;649:123644. doi:10.1016/j.ijpharm.2023.123644
17. Lelli D, Sahebkar A, Johnston TP, Pedone C. Curcumin use in pulmonary diseases: state of the art and future perspectives. *Pharmacol Res*. 2017;115:133–148. doi:10.1016/j.phrs.2016.11.017
18. Sharma RA, Euden SA, Platton SL, et al. Phase I clinical trial of oral curcumin: biomarkers of systemic activity and compliance. *Clin Cancer Res*. 2004;10:6847–6854. doi:10.1158/1078-0432.Ccr-04-0744
19. Lao CD, Ruffin MTT, Normolle D, et al. Dose escalation of a curcuminoid formulation. *BMC Complement Altern Med*. 2006;6:10. doi:10.1186/1472-6882-6-10
20. Sabet S, Rashidinejad A, Melton LD, McGillivray DJ. Recent advances to improve curcumin oral bioavailability. *Trend Food Sci Technol*. 2021;110:253–266. doi:10.1016/j.tifs.2021.02.006
21. Dallinger C, Trommeshauser D, Marzin K, Liesener A, Kaiser R, Stopfer P. Pharmacokinetic properties of nintedanib in healthy volunteers and patients with advanced cancer. *J Clin Pharmacol*. 2016;56:1387–1394. doi:10.1002/jcph.752
22. Zhu Y, Fu Y, Zhang A, et al. Rod-shaped nintedanib nanocrystals improved oral bioavailability through multiple intestinal absorption pathways. *Eur J Pharm Sci*. 2022;168:106047. doi:10.1016/j.ejps.2021.106047
23. Liu S, Chen H, Zhou F, et al. Characterization and evaluation of nintedanib amorphous solid dispersions with enhanced oral bioavailability. *AAPS PharmSciTech*. 2024;25:183. doi:10.1208/s12249-024-02902-x
24. Silva AC, Costa MP, Zacaron TM, et al. The role of inhaled chitosan-based nanoparticles in lung cancer therapy. *Pharmaceutics*. 2024;16:969. doi:10.3390/pharmaceutics16080969
25. He Y, Liang Y, Mak JCW, et al. Size effect of curcumin nanocrystals on dissolution, airway mucosa penetration, lung tissue distribution and absorption by pulmonary delivery. *Colloids Surf B*. 2020;186:110703. doi:10.1016/j.colsurfb.2019.110703
26. Lee C, Seo J, Hwang HS, et al. Treatment of bleomycin-induced pulmonary fibrosis by inhaled tacrolimus-loaded chitosan-coated poly(lactic-co-glycolic acid) nanoparticles. *Biomed Pharmacother*. 2016;78:226–233. doi:10.1016/j.biopha.2016.01.027
27. Chen X, Gu J, Sun L, et al. Efficient drug delivery and anticancer effect of micelles based on vitamin E succinate and chitosan derivatives. *Bioactive Materials*. 2021;6:3025–3035. doi:10.1016/j.bioactmat.2021.02.028
28. Balogun-Agbaje OA, Odeniyi OA, Odeniyi MA. Drug delivery applications of poly-γ-glutamic acid. *Fut J Pharm Sci*. 2021;7:125. doi:10.1186/s43094-021-00280-w
29. Xin X, Yao D, Zhang K, et al. Protective effects of Rosavin on bleomycin-induced pulmonary fibrosis via suppressing fibrotic and inflammatory signaling pathways in mice. *Biomed Pharmacother*. 2019;115:108870. doi:10.1016/j.biopha.2019.108870
30. Qi D, Jia B, Peng H, et al. Baicalin/ambroxol hydrochloride combined dry powder inhalation formulation targeting lung delivery for treatment of idiopathic pulmonary fibrosis: fabrication, characterization, pharmacokinetics, and pharmacodynamics. *Eur J Pharm Biopharm*. 2023;188:243–253. doi:10.1016/j.ejpb.2023.05.017
31. Hegde M, Girisa S, BharathwajChetty B, Vishwa R, Kunnumakkara AB. Curcumin formulations for better bioavailability: what we learned from clinical trials thus far? *ACS Omega*. 2023;8:10713–10746. doi:10.1021/acsomega.2c07326
32. Liu H, Du K, Li D, et al. A high bioavailability and sustained-release nano-delivery system for nintedanib based on electrospray technology. *Int J Nanomedicine*. 2018;13:8379–8393. doi:10.2147/ijn.S181002
33. Milara J, Ballester B, Safont MJ, et al. MUC4 is overexpressed in idiopathic pulmonary fibrosis and collaborates with transforming growth factor β inducing fibrotic responses. *Mucosal Immunol*. 2021;14:377–388. doi:10.1038/s41385-020-00343-w
34. Ashley SL, Wilke CA, Kim KK, Moore BB. Periostin regulates fibrocyte function to promote myofibroblast differentiation and lung fibrosis. *Mucosal Immunol*. 2017;10:341–351. doi:10.1038/mi.2016.61
35. Boutanquoi PM, Burgy O, Beltramo G, et al. TRIM33 prevents pulmonary fibrosis by impairing TGF-β1 signalling. *Eur Respir J*. 2020;55:1901346. doi:10.1183/13993003.01346-2019
36. Ma WH, Li M, Ma HF, et al. Protective effects of GHK-Cu in bleomycin-induced pulmonary fibrosis via anti-oxidative stress and anti-inflammation pathways. *Life Sci*. 2020;241:117139. doi:10.1016/j.lfs.2019.117139
37. Liu Y, Zhou P, Cao Z, et al. Simultaneous solubilization and extended release of insoluble drug as payload in highly soluble particles of γ-cyclodextrin metal-organic frameworks. *Int J Pharm*. 2022;619:121685. doi:10.1016/j.ijpharm.2022.121685
38. Yang F, Hou ZF, Zhu HY, et al. Catalpol protects against pulmonary fibrosis through inhibiting TGF-β1/Smad3 and Wnt/β-Catenin signaling pathways. *Front Pharmacol*. 2020;11:594139. doi:10.3389/fphar.2020.594139